ISSN 0957-4484

NANOTECHNOLOGY

VOLUME 23 NUMBER 34 31 AUGUST 2012

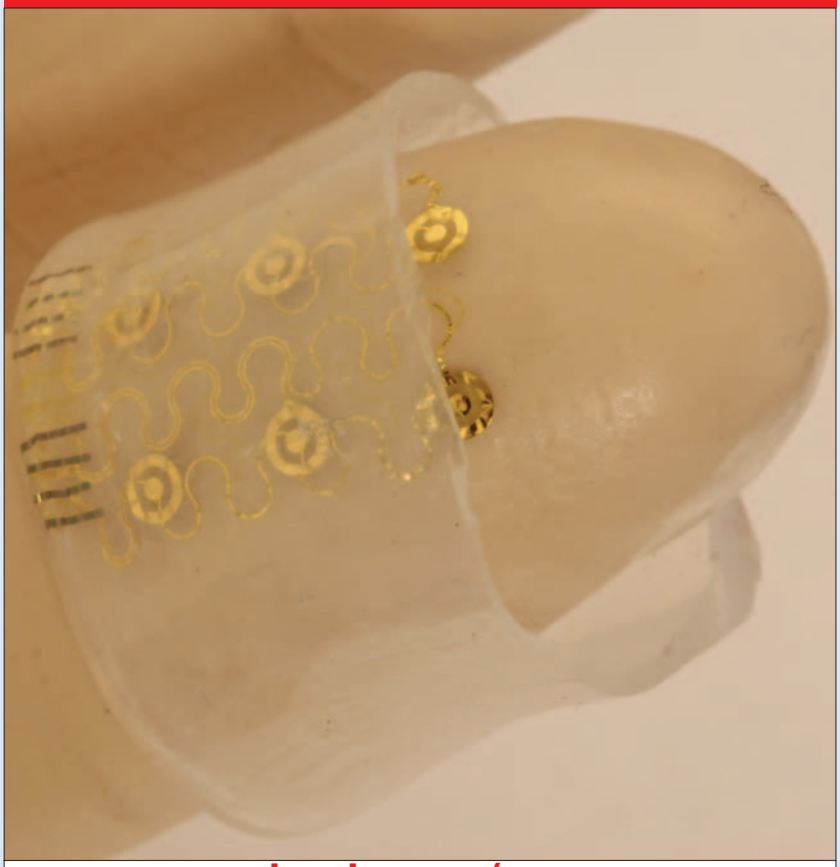

iopscience.org/nano

Special issue
Nanotechnology-based flexible electronics

IOP Publishing

Silicon nanomembranes for fingertip electronics

2012 Nanotechnology 23 344004

(http://iopscience.iop.org/0957-4484/23/34/344004)

Nanotechnology **23** (2012) 344004 (7pp) doi:10.1088/0957-4484/23/34/344004

Silicon nanomembranes for fingertip electronics

Ming Ying[1,4], Andrew P Bonifas[1,4], Nanshu Lu[1], Yewang Su[2], Rui Li[2,3], Huanyu Cheng[2], Abid Ameen[1], Yonggang Huang[2] and John A Rogers[1]

[1] Department of Materials Science and Engineering, Frederick Seitz Materials Research Laboratory, University of Illinois at Urbana-Champaign, Urbana, IL 61801, USA
[2] Department of Mechanical Engineering and Department of Civil and Environmental Engineering, Northwestern University, Evanston, IL 60208, USA
[3] Faculty of Infrastructure Engineering, Dalian University of Technology, Dalian 116024, People's Republic of China

E-mail: jrogers@uiuc.edu

Received 3 February 2012, in final form 8 March 2012
Published 10 August 2012
Online at stacks.iop.org/Nano/23/344004

Abstract
We describe the use of semiconductor nanomaterials, advanced fabrication methods and unusual device designs for a class of electronics capable of integration onto the inner and outer surfaces of thin, elastomeric sheets in closed-tube geometries, specially formed for mounting on the fingertips. Multifunctional systems of this type allow electrotactile stimulation with electrode arrays multiplexed using silicon nanomembrane (Si NM) diodes, high-sensitivity strain monitoring with Si NM gauges, and tactile sensing with elastomeric capacitors. Analytical calculations and finite element modeling of the mechanics quantitatively capture the key behaviors during fabrication/assembly, mounting and use. The results provide design guidelines that highlight the importance of the NM geometry in achieving the required mechanical properties. This type of technology could be used in applications ranging from human–machine interfaces to 'instrumented' surgical gloves and many others.

S Online supplementary data available from stacks.iop.org/Nano/23/344004/mmedia

(Some figures may appear in colour only in the online journal)

1. Introduction

Electrotactile stimulators and tactile sensors are of interest as bi-directional information links between a human operator and a virtual environment, in a way that could significantly expand function in touch-based interfaces to computer systems, with applications in simulated surgery, therapeutic devices, robotic manipulation, and others [1–5]. Electrotactile stimulation allows information to be presented through the skin, as an artificial sensation of touch, commonly perceived as a vibration or tingling feeling [6, 7]. Such responses are manifested through the excitation of cutaneous mechanoreceptors as a result of passage of a suitably modulated electrical current into the tissue [8]. Developed originally in the 1950s and further advanced in the 1970s, electrotactile stimulation has been traditionally explored for programmable braille readers and displays for the visually impaired as well as for balance control in individuals who suffer from vestibular disorders [5, 9–12]. Tactile sensors, on the other hand, measure the pressure created by physical contact, in a way that provides complementary information for potential use in feedback loops with the electrotactile process. Additional classes of sensors that can be important in this context include those for motion and temperature. Incorporation of such technologies into a conformal, skin-like device capable of intimate, non-invasive mounting on the fingertips might, therefore, represent a useful achievement. Recent advances in flexible and stretchable electronics create opportunities to build this type of device [13–17].

Here we report materials, fabrication strategies and device designs for ultrathin, stretchable silicon-based electronics and sensors that can be mounted on the inner

[4] These authors contributed equally to this work.

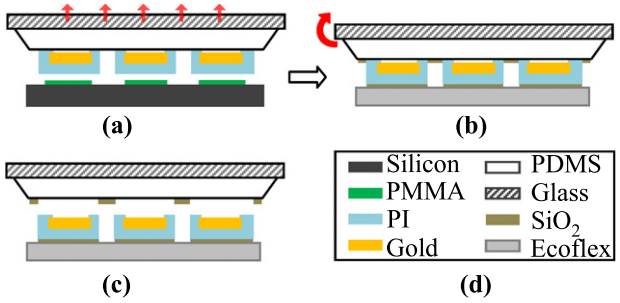

Figure 1. Schematic illustration of the process for transfer printing an interconnected device structure from a substrate on which it is fabricated to an elastomeric sheet. (a) Interconnected sensors and electronics formed on a silicon wafer in an open mesh geometry are lifted onto the surface of a PDMS slab (i.e. stamp); (b) the back side of the mesh and the supporting PDMS stamp are coated with a thin layer of SiO_2 and then pressed onto an elastomeric sheet (Ecoflex); (c) removal of the PDMS completes the transfer; (d) materials legend.

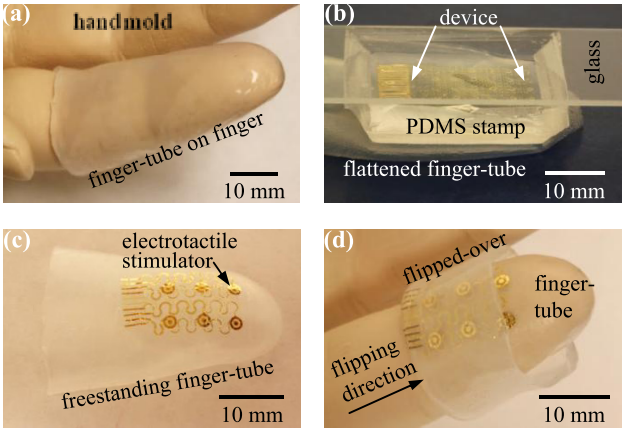

Figure 2. The process for fabricating a multiplexed array of electrotactile stimulators in a stretchable, mesh geometry on the inner surface of an elastomeric finger-tube. (a) Casting and curing an elastomer precursor on the finger of a model hand yields a thin (∼500 μm thick), closed-form membrane, i.e. a finger-tube; (b) a PDMS stamp (here backed by a glass microscope slide) delivers the electrotactile device to the outer surface of this finger-tube, while compressed into a flattened geometry; (c) electrotactile array on the outside of the freestanding finger-tube; (d) turning the tube inside out relocates the array on the inner surface of the finger-tube, shown here at the midway point of this flipping process.

and outer surfaces of elastomeric closed-tube structures for integration directly on the fingertips. The active components and interconnects incorporate advanced mechanics designs, capable of accommodating large strains induced not only by natural deformations of the tubes during use, but also during a critical step in the fabrication process in which the tubes, specially formed to match the shapes of fingertips, are flipped inside out. This 'flipping-over' process allows devices initially mounted on the outer surface of the tube to be reversed to the inner surface, where they can press directly against the skin when mounted on the fingers. Analytical calculations and finite element modeling (FEM) provide quantitative insights into design layouts that avoid plastic deformation or fracture. We demonstrate these concepts in multifunctional fingertip devices that include electrotactile electrode arrays multiplexed with Si nanomembrane (NM) diodes, strain sensors based on Si NM gauges, and tactile sensor arrays that use capacitors with low modulus, elastomeric dielectrics.

2. Experiments

Figure 1 schematically illustrates the steps for integrating devices based on Si NMs in stretchable, interconnected geometries with elastomeric substrates, following adapted versions of procedures described elsewhere [13, 18]. (Details appear in the supplementary file available at stacks.iop.org/Nano/23/344004/mmedia.) The fabrication uses a Si wafer with a 100 nm thick coating of polymethylmethacrylate (PMMA) as a temporary substrate for the initial parts of the process. A layer of polyimide (PI, 1.25 μm thick) formed by spin coating a poly (amic acid) precursor and baking in an inert atmosphere at 250 °C serves as the support for the devices. Electronically active materials are deposited (e.g. metallization) or transfer printed (e.g. Si NMs) onto the PI and patterned by photolithography and etching. (Details appear in the supplementary file available at stacks.iop.org/Nano/23/344004/mmedia.) Another layer of PI (1.25 μm thick) spin cast and cured on top of the device layers provides encapsulation and locates the devices near the neutral mechanical plane (NMP). Next, patterned reactive ion etching through the entire multilayer stack (i.e. PI/devices/PI) defines an open mesh structure. This same process removes the PI in the regions of the electrotactile stimulation electrodes, to allow direct contact with the skin. Immersion in an acetone bath washes away the underlying PMMA, thereby allowing the entire mesh to be lifted off, in a single piece, onto the surface of a flat slab of polydimethylsiloxane (PDMS), using procedures described previously [19, 20]. Evaporation of a layer of SiO_2 onto the mesh/PDMS and exposure of the silicone target substrate (Ecoflex 0030, Smooth-On, Inc.) to UV–ozone (to create reactive –OH groups on the surface) enables bonding between the two upon physical contact [21]. (Low pressures avoid contact between the PDMS and the finger-tube, thereby allowing bonding only to the mesh.) The SiO_2 adhesion layer does not serve any electronic function. Removal of the stamp completes the transfer process, as shown in figure 1(c).

The electrotactile electrodes use 600 nm thick layers of Au in a concentric design, consisting of an inner disk (400 μm radius) surrounded by an outer ring (1000 μm radius) with a 250 μm wide gap between the two. The interconnects consist of 100 μm wide traces of Au in serpentine geometries (radii of curvature ∼ 800 μm); these traces connect the electrotactile electrodes to Si NM diodes (lateral dimensions of 225 μm × 100 μm and thicknesses of 300 nm). Two layers of Au interconnects (200 and 600 nm thick), isolated by a 1.25 μm PI layer and connected through etched PI vias, establish a compact wiring scheme with overlying interconnects. The 600 nm thick Au interconnect layer allows robust electronic contact though the PI vias. The strain gauge arrays consist of four Si NMs (strips with lateral dimensions of 1 mm × 50 μm and thicknesses of

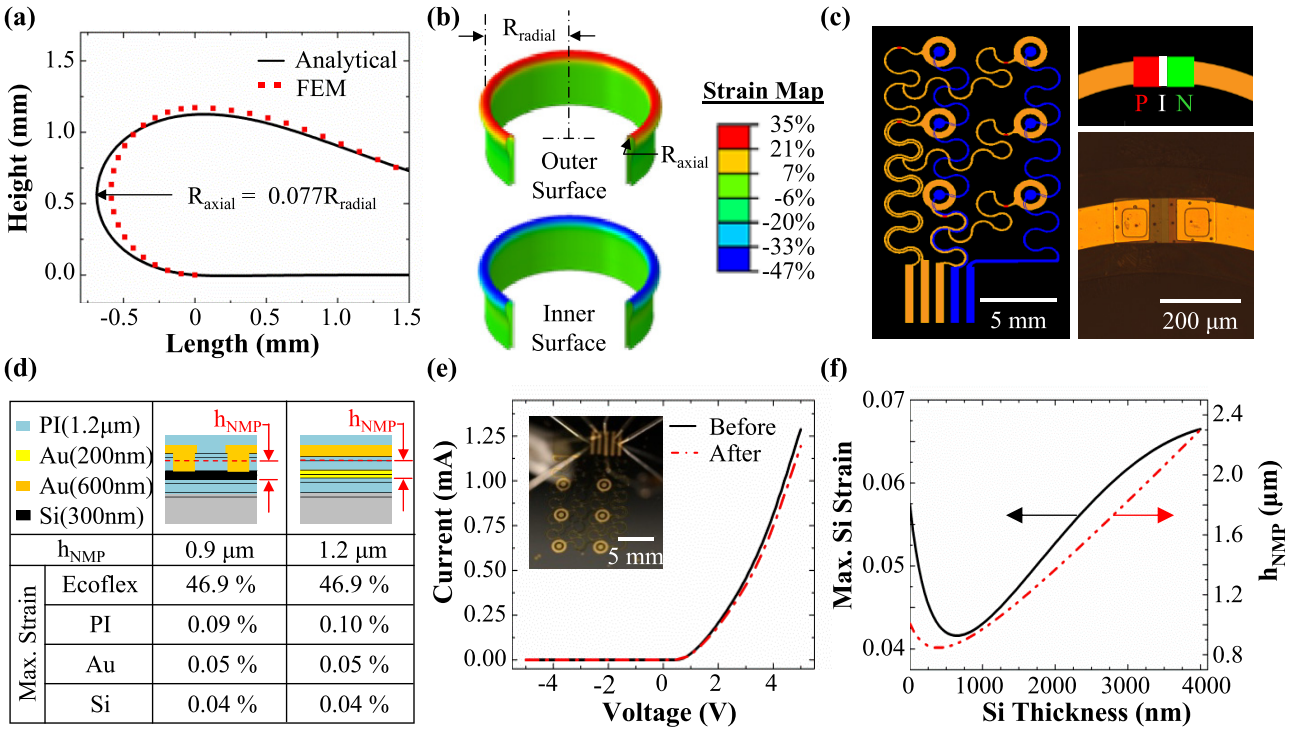

Figure 3. Mechanics modeling of the 'flipping-over' process and application to arrays of electrotactile stimulators multiplexed with Si NM diodes. (a) Calculated (analytical and FEM) profiles of an Ecoflex finger-tube during bending associated with flipping the tube inside out, showing the relationship between the radius (R_{radial} = 7.5 mm) of the tube and the minimum bending radius (R_{axial}); (b) FEM results for maximum strains on the inner and outer surfaces during this process; (c) schematic illustration of a multiplexed electrotactile array with serpentine mesh interconnects, with a magnified diagram (right top) and an image (right bottom) of a PIN Si NM diode (after flipping over); (d) schematic cross sectional illustrations of two regions of the device, with the position of the NMP indicated by a dashed red line, and analytical results for the maximum strains during the flipping-over process; (e) *I–V* characteristics of a Si NM diode before and after flipping over; (f) maximum strain in the Si NM diode and h_{NMP} (the offset between the neutral mechanical plane and the lower surface of the Si NM) as a function of the thickness of the Si NM.

300 nm) electrically connected by 200 nm thick, 60 μm wide Au traces patterned in serpentine shapes (radii of curvature $\sim$ 400 μm). The tactile sensors use 200 nm thick Au electrodes and interconnects in the geometry of the electrotactile arrays but with the concentric electrode pairs replaced by single, disk-shaped electrodes (radii $\sim$ 1000 μm).

The Ecoflex substrates, which we refer to as finger tubes, adopt three-dimensional forms specifically matched to those of fingers on a plastic model of the hand. The fabrication involves pouring a polymer precursor to Ecoflex onto a finger of the model and curing at room temperature for 1 h, to create a conformal sheet with $\sim$125 μm thickness. Pouring a second coating of precursor onto this sheet and curing for an additional 1 h doubles the thickness; repeating this process four times results in a thickness of $\sim$500 μm. Removing the Ecoflex from the model and completing the cure by heating at 70 °C for 2 h forms a free standing structure, i.e. a finger-tube, like the one illustrated in figure 2. Ecoflex is an attractive material for this purpose because it has a low modulus ($\sim$60 kPa) and large fracture strain ($\sim$900%). The former allows soft, intimate contact with the skin; the latter enables the 'flipping-over' process referred to previously, and described in quantitative detail in section 3. Transfer printing delivers the device mesh structure to the outer surface of the finger-tube, while pressed into a flattened geometry (figure 2(b)). The entire integrated system is then flipped inside out, to move the mesh from the outer to the inner surface of the tube, as shown in figures 2(c) and (d). Multifunctional devices incorporate electrotactile stimulators on the inside, and strain gauge arrays and tactile sensors on the outside.

3. Results and discussion

The device designs described previously have the advantage that they are conformal to the finger, in a way that naturally presses the electronics on the interior surface of the finger-tube (in this case the electrotactile stimulating electrodes) into intimate contact with the skin. The flipping-over process represents a critical step, enabled by careful design of the mechanics in the device mesh. Quantitative mechanics modeling provides important insights. The finger-tube can be approximated as a self-equilibrated, axisymmetric tube with two-dimensional symmetry. Energy minimization using linear elastic shell theory determines the resulting shapes. Figure 3(a) shows analytical and FEM results for an Ecoflex cylinder with a radius (R_{radial}) of 7.5 mm and a thickness of 500 μm when bent back on itself, at a midway point during the flipping-over process. The minimum axial radius of curvature (R_{axial}) of 596 μm, as indicated in figure 3(a), defines the location of maximum induced strain as the tube is flipped over.

The maximum strains on the inner and outer surfaces in this configuration, as shown in the color map of figure 3(b), are ∼30–40% (see supplementary file at stacks.iop.org/Nano/23/344004/mmedia). The device mesh structures must, therefore, be able to accommodate strains in this range. This requirement is non-trivial for systems like the ones described here, due to their incorporation of brittle materials such as silicon (fracture strain ∼ 1%).

Circuit layouts, guided by theory, can be identified to satisfy these requirements. As an example, figure 3(c) provides a diagram of a multiplexed electrotactile array in a mesh configuration with narrow, serpentine interconnects. The orange and blue regions correspond to Au layers separated by layers of PI, respectively; the red regions indicate Si NM (300 nm thick) diodes in a PIN (p-doped/intrinsic/n-doped) configuration. The short dimensions of the diodes lie parallel to the flipping-over direction, to minimize the strains in the Si during this process. These optimizations lead to maximum calculated strains that are only 0.051%, 0.10%, and 0.040% for the Au, PI, and the Si, respectively (see figure 3(d) and supplementary file available at stacks.iop.org/Nano/23/344004/mmedia). The computed position of the NMP also appears in figure 3(d). Since the moduli of the device layers are several orders of magnitude larger than that of Ecoflex, the location of the NMP plane is largely independent of the Ecoflex. Appropriate selection of the thicknesses of the PI layers allows the NMP to be positioned at the location of the Si NMs, thereby minimizing the induced strains in this brittle material [21, 22]. The thicknesses of the Si NM diodes influence the maximum strains that they experience, as shown in the analytical calculations of figure 3(f). A minimum occurs at the thickness that places the NMP at the shortest distance from the Si NM diode (i.e. h_{NMP}). The position of this minimum can also be adjusted by changing the thicknesses of the PI layers, for example. Further reductions in strain can be realized by reducing the lengths of the devices. Implementation of designs that incorporate these considerations and together with the use of interconnects with optimized serpentine layouts ensure robust device behavior throughout the fabrication sequence. For example, figure 3(e) shows negligible change in the *I*–*V* characteristics (Agilent 4155C semiconductor parameter analyzer) of a Si NM diode before and after the flipping-over process.

The experimental results demonstrate the expected functionality in the electrotactile arrays. Figure 4(a) shows the perception of touch on a dry human thumb as a function of voltage and frequency, applied between the inner dot and outer ring electrodes (figure 3(c)). The stimulation used a monophasic, square wave with 20% duty cycle, generated using a custom setup. The inset provides an image of a device, with connection to external drive electronics via a flexible anisotropic conductive film (ACF). The required voltage for sensation decreases with increasing frequency, consistent with equivalent circuit models of skin impedance that involve resistors and capacitors connected in parallel. The absolute magnitudes of these voltages depend strongly on the skin hydration level, electrode design, and stimulation waveform [23]. Figure 4(b) shows *I*–*V* characteristics of an

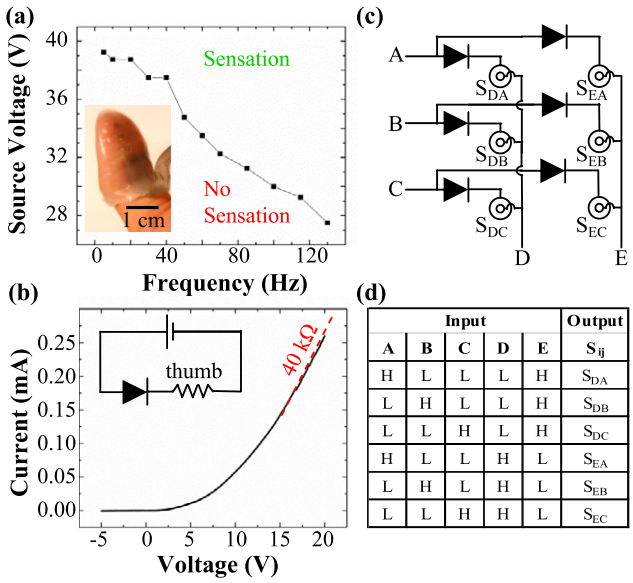

(d)

Input					Output
A	B	C	D	E	S_{ij}
H	L	L	L	H	S_{DA}
L	H	L	L	H	S_{DB}
L	L	H	L	H	S_{DC}
H	L	L	H	L	S_{EA}
L	H	L	H	L	S_{EB}
L	L	H	H	L	S_{EC}

Figure 4. Mechanics and electrical characteristics of a 2 × 3, multiplexed electrotactile array on a finger-tube. (a) Voltage required for electrotactile sensation as a function of stimulation frequency; inset: electrotactile array on a human finger during experiments; (b) *I*–*V* characteristics of multiplexed electrotactile electrodes in contact with a human thumb; (c) circuit diagram of the diode multiplexing scheme; (d) function table showing inputs for addressing each of the six channels (H = high; L = low).

electrotactile electrode pair while in contact with a hydrated human thumb, measured through a multiplexing diode. At high positive voltages, the resistance of the diode is negligible compared to the skin; here, the slope of the *I*–*V* characteristics yield an estimate of the resistance of the skin–electrode contact plus the skin. The value (∼40 kΩ) is in a range consistent with measurements using conventional devices [24, 25]. The diode is stable to at least 20 V, corresponding to currents of 0.25 mA, which is sufficient for electrotactile stimulation on the skin and tongue [2, 6, 7].

These diodes enable multiplexed addressing, according to an approach that appears schematically in figure 4(c). Each unit cell consists of one diode and one electrotactile electrode pair. Figure 4(d) presents a table of the inputs required to address each of the six electrotactile channels. For example, channel S_{DA} can be activating by applying a high potential (+5 V) to inputs A and E and a low potential (0 V) to inputs B, C, and D, thereby yielding a +5 V bias across the outer ring (+5 V) and inner ring electrodes (0 V) of this channel. This configuration forward biases the Si NM diode, which results in a stimulation current, as shown in figure 4(b). At the same time, channels S_{EB} and S_{EC} experience a bias of −5 V across the electrodes but in these cases the Si NM diodes are reverse biased, thus preventing a stimulating current. Channels S_{DB}, S_{DC}, and S_{EA} have the same potentials on the inner and outer electrodes, resulting in zero bias. Electrical isolation of adjacent channels is a consequence of inner to outer electrode separations (250 μm) that are small compared to the distances between channels (6000 μm). Advanced multiplexing schemes that use several diodes per

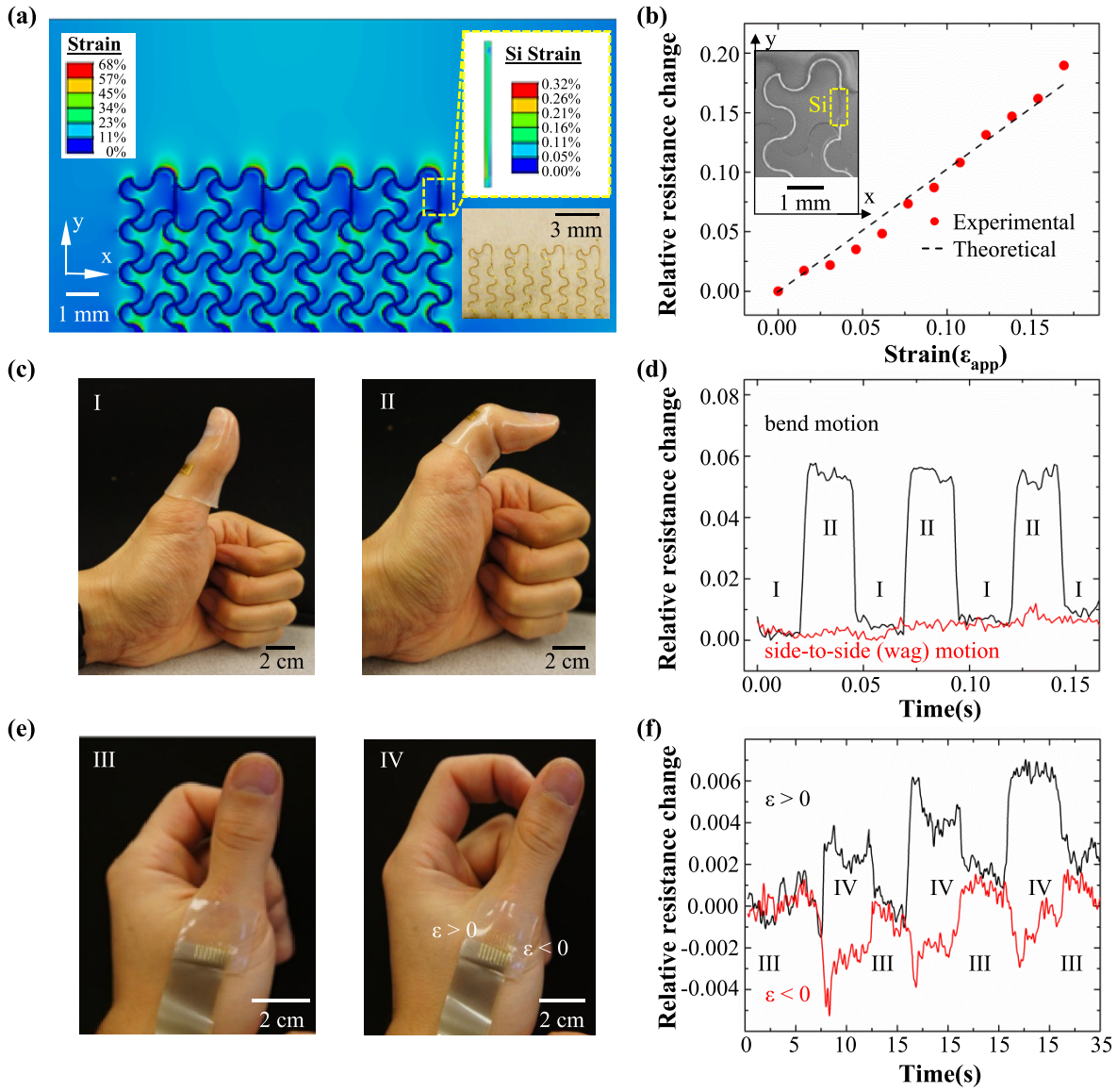

Figure 5. Detection of finger motion with arrays of stretchable Si NM strain gauges. (a) FEM results of the maximum principal strain for a 1×4 array of gauges (straight, vertical structures near the top of the serpentine interconnect mesh) due to an overall 10% strain applied along the longitudinal (y) direction. The upper inset shows the strains in the gauge highlighted by the yellow dashed box. The lower inset provides an image of a fabricated device with a layout that matches that of the FEM results. (b) Experimentally measured and analytically calculated changes in resistance for a representative Si NM strain gauge as a function of applied strain along the longitudinal direction. The inset provides an SEM image of a portion of the device, with the Si NM gauge located in the dashed box. (c) Images of a strain gauge array on a finger-tube mounted on the thumb, in straight (I) and bent (II) positions. (d) Change in resistance of a representative gauge during three bending cycles (black) and side-to-side motion (red). (e) Images of a strain gauge array on a thin, elastomeric sheet laminated onto the metacarpal region of the thumb in straight (III) and sideways deflected (IV) positions. (f) Change in resistance of gauges at two ends of the array during three cycles of side-to-side motion.

stimulation channel, or active transistors, are compatible with the fabrication process and design principles outlined here.

Figure 5 shows a set of straight, uniformly doped Si NMs as strain gauges addressed with interconnects in a mesh geometry. The FEM calculations summarized in figure 5 reveal the strain profiles in a 1×4 array of gauges (vertical strips; the yellow dashed box in the upper inset highlights an individual device) on Ecoflex, under a uniaxial in-plane strain of 10%. These results show that the overall strain is mostly accommodated by changes in the shapes of the serpentine interconnects and, of course, the Ecoflex itself. The Si NM gauges experience strains ($\sim 10^{-3}$) that are ten times lower than the applied strain, as shown in the inset in figure 5(a).

The ability to use Si NMs as high performance strain gauges in stretchable forms results from the strong piezoresistance properties of Si, combined with serpentine layouts. These characteristics, taken together, determine the fractional change in resistance per applied strain. The associated effective gauge factor (GF_{eff}) can be related to the intrinsic gauge factor of a silicon gauge, $GF_{Si} = \Delta R/(R\varepsilon_{Si})$, where ΔR is the change in resistance, R is the initial resistance, and ε_{Si} is the strain in the silicon, by

the following expression: $GF_{eff} = GF_{Si}$ $(\varepsilon_{Si}/\varepsilon_{app})$, where ε_{app} is the strain applied to the overall, integrated system. The designs reported here yield values of $\varepsilon_{Si}/\varepsilon_{app}$ that are much smaller than one, specifically to avoid fracture-inducing strains in the Si during fabrication, mounting and use over physiologically relevant ranges of strain. Figure 5(b) shows experimentally measured values of $\Delta R/R$ (evaluation at 1 V, using an Agilent 4155C semiconductor parameter analyzer) as a function of ε_{app}, which corresponds to $GF_{eff} \sim 1$. By fitting the experimental and FEM results to figure 5(b), the GF_{Si} is ∼95, consistent with a recent report on Si NM strain gauges, with otherwise similar designs, on flexible sheets of plastic [26]. We emphasize that the device parameters, such as the size of the gauge and the dimensions of the serpentine interconnects, enable engineering control over GF_{eff}, from values as large as GF_{Si} to those that are much smaller, with a correspondingly increased range of strains over which measurements are possible.

Figure 5(c) shows a strain gauge array on a finger-tube located near the knuckle region of the thumb, in straight (I) and bent (II) positions. Upon bending, the gauges experience tensile strain, resulting in an increase in resistance, as shown for three bending cycles in figure 5(d). The relative resistance changes suggest that the strain associated with bending reaches ∼6%. As expected, side-to-side motions induce no changes. Figure 5(e) highlights a similar array on a thin sheet of Ecoflex, mounted near the metacarpal region of the thumb. Here, the device adheres to the skin by van der Waals interactions, similar to the mechanisms observed in epidermal electronic systems [13]. The images in figure 5(e) correspond to the thumb in straight (III) and sideways deflected (VI) positions. The changes in resistance for the two gauges on opposite ends of the 1 × 4 array for three side-to-side cycles of motion appear in figure 5(f). For each cycle, the change in resistance of the rightmost gauge indicates compressive strain; the leftmost indicates the corresponding tensile strain. The results suggest that arrays of gauges can be used to identify not only the magnitude but also the type of motion.

As a final demonstration, we built a type of tactile (pressure) sensor suitable for integration on the finger-tube platform. The devices exploit changes in capacitance associated with opposing electrodes on the inner and outer surfaces of the Ecoflex. Applied pressure decreases the thickness of the Ecoflex, thereby increasing the capacitance of this structure. Here, layouts like those for the electrotactile devices serve as inner electrodes; a mirror image of this array mounted in an aligned configuration on the outer surface defines a collection of parallel plate capacitors with the Ecoflex as the dielectric. An array of such devices on the anterior surface of a model of the hand appears in figure 6(a). Figures 6(b) and (c) show images of the inner and outer electrode arrays. The relative change in capacitance with applied pressure for a representative device appears in figure 6(d) (black symbols). Here, the capacitance was measured (Agilent E4980A LCR meter) as a function of the pressure applied with a series of weights mounted on a platform with a constant contact area, taking care to minimize the effects of parasitic capacitances and to eliminate ground

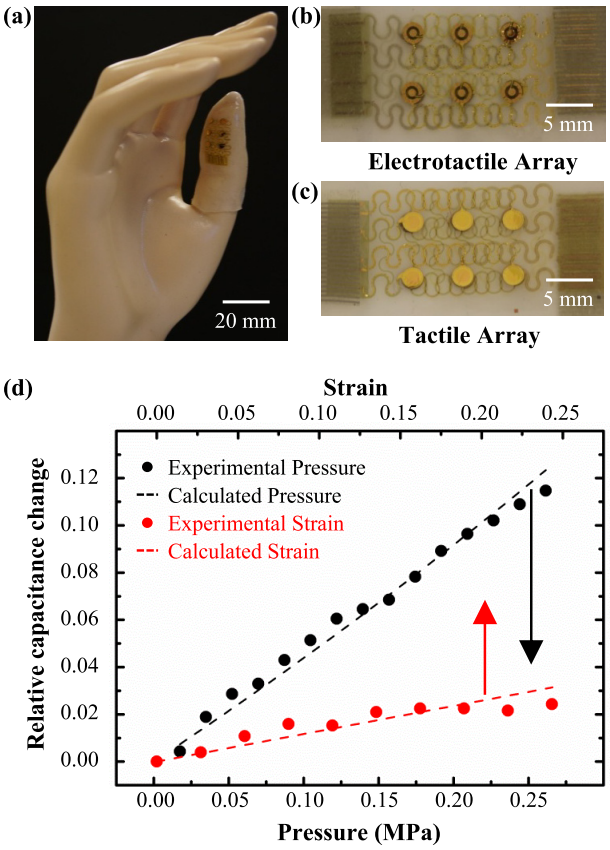

Figure 6. Tactile sensing with integrated capacitance sensors. (a) Sensors on the anterior of the thumb; (b) inner electrodes for a 2 × 3 array of sensors (electrotactile electrodes); (c) outer electrodes for the same array; (d) measured and analytically calculated change in capacitance of a single sensor with applied pressure and tensile strain.

loops. Approximately linear behavior is observed over the range studied, consistent with a simple mechanical model, $\Delta C/C_o = P/(\bar{E}_{Ecoflex} - P)$, where ΔC is the capacitance change, C_o is the initial capacitance, P is the applied pressure, and $\bar{E}_{Ecoflex}$ is the effective Ecoflex modulus. This simple model assumes no electrostriction or strain induced changes in the dielectric constant (figure 6(d), black line). Due to the Poisson effect, the devices also respond to in-plane strains ($\varepsilon_{applied}$), as shown in figure 6(d) (red), consistent with the simple model $\Delta C/C_o = [(EA)_{system}/(EA)_{electrodes}]\nu\varepsilon_{applied}$, where the Poisson's ratio ν is 0.496, and $(EA)_{system}$ and $(EA)_{electrodes}$ are the tensile stiffnesses of the system and the electrodes respectively (see supplementary file available at stacks.iop.org/Nano/23/344004/mmedia). This type of technology provides a simple alternative to recently reported devices that offer similar functionality, but on flexible substrates, and based on conductive elastomers, elastomeric dielectrics, or compressible gate dielectrics in organic transistors [14, 16, 18, 27, 28].

4. Summary and conclusion

The results presented here establish some procedures and design rules for electronics and sensors that can be mounted conformally onto the fingers. Other appendages of the body

can be addressed in a similar manner. Furthermore, most of the considerations in the mechanics and fabrication are agnostic to the specific device functionality or mounting locations. As a result, many of these concepts can be applied generally, to other types of system and modes of use. Future challenges include the development of capabilities for wireless power supply and data transfer.

Acknowledgments

This work was carried out in part at the Fredrick Seitz Materials Research Laboratory Central Facilities, University of Illinois, which are partially supported by the US Department of Energy under grants DE-FG02-07ER46453 and DE-FG02-07ER46471. The work was also supported by a National Security Science and Engineering Fellowship and the Center for Nanoscale Chemical Electrical Mechanical Manufacturing Systems at the University of Illinois, which was funded by the National Science Foundation under grant CMMI-0328162. Y H acknowledges support from NSF Grant Nos ECCS-0824129 and OISE-1043143. The authors would like to gratefully acknowledge Yun Soung Kim for helping with the silicon transfer printing, Yizhu Xie for his assistance with the silicon doping, Camille Goudeseune for providing the control circuit and programming for electrotactile stimulation, and Xian Huang for technical discussion.

References

[1] Barfield W, Hendrix C, Bjorneseth O, Kaczmarek K A and Lotens W 1995 *Presence-Teleop. Virt.* **4** 329
[2] Matteau I, Kupers R, Ricciardi E, Pietrini P and Ptito M 2010 *Brain Res. Bull.* **82** 264
[3] Tan H Z, Durlach N I, Reed C M and Rabinowitz W M 1999 *Percept. Phychophys.* **61** 993
[4] Sparks D W, Kuhl P K, Edmonds A E and Gray G P 1978 *J. Acoust. Soc. Am.* **63** 246
[5] Danilov Y P, Tyler M E and Kaczmarek K A 2008 *Int. J. Psychophysiol.* **69** 162
[6] Kaczmarek K A, Webster J G, Bachyrita P and Tompkins W J 1991 *IEEE Trans. Biomed. Eng.* **38** 17
[7] Lozano C A, Kaczmarek K A and Santello M 2009 *Somatosens. Mot. Res.* **26** 50
[8] Warren J P, Bobich L R, Santello M, Sweeney J D and Tillery S I H 2008 *IEEE Trans. Neural Syst. Rehabil.* **16** 410
[9] Bach-y-Rita P, Tyler M E and Kaczmarek K A 2003 *Int. J. Hum.-Comput. Int.* **15** 285
[10] Jones L A and Safter N B 2008 *Hum. Factors* **50** 90
[11] Vuillerme N, Pinsault N, Chenu O, Demongeot J, Payan Y and Danilov Y 2008 *Neurosci. Lett.* **431** 206
[12] Vidal-Verdu F and Hafez M 2007 *IEEE Trans. Neural Syst. Rehabil.* **15** 119
[13] Kim D H *et al* 2011 *Science* **333** 838
[14] Lipomi D J, Vosgueritchian M, Tee B C, Hellstrom S L, Lee J A, Fox C H and Bao Z 2011 *Nature Nanotechnol.* **6** 788
[15] Rogers J A and Huang Y G 2009 *Proc. Natl Acad. Sci. USA* **106** 10875
[16] Someya T, Sekitani T, Iba S, Kato Y, Kawaguchi H and Sakurai T 2004 *Proc. Natl Acad. Sci. USA* **101** 9966
[17] Rogers J A, Lagally M G and Nuzzo R G 2011 *Nature* **477** 45
[18] Kim D H *et al* 2011 *Nature Mater.* **10** 316
[19] Meitl M A *et al* 2006 *Nature Mater.* **5** 33
[20] Yu J and Bulovic V 2007 *Appl. Phys. Lett.* **91** 043102
[21] Kim D H *et al* 2008 *Science* **320** 507
[22] Rogers J A, Someya T and Huang Y G 2010 *Science* **327** 1603
[23] Kaczmarek K A and Haase S J 2003 *IEEE Trans. Neural Syst. Rehabil.* **11** 9
[24] Woo E J, Hua P, Webster J G, Tompkins W J and Pallasareny R 1992 *Med. Biol. Eng. Comput.* **30** 97
[25] Hua P, Woo E J, Webster J G and Tompkins W J 1993 *IEEE Trans. Biomed Eng.* **40** 335
[26] Won S M *et al* 2011 *IEEE Trans. Electron Devices* **58** 4074
[27] Someya T *et al* 2005 *Proc. Natl Acad. Sci. USA* **102** 12321
[28] Takei K *et al* 2010 *Nature Mater.* **9** 821

Silicon Nanomembranes for Fingertip Electronics

Supplementary Data

Ming Ying[1*]

Andrew P. Bonifas[1*]

Nanshu Lu[1]

Yewang Su[2]

Rui Li[3,2]

Huanyu Cheng[2]

Abid Ameen[1]

Yonggang Huang[2]

John A. Rogers[1†]

1. Department of Materials Science and Engineering, Frederick Seitz Materials Research Laboratory, University of Illinois at Urbana-Champaign, Urbana, IL 61801, USA.

2. Department of Mechanical Engineering and Department of Civil and Environmental Engineering, Northwestern University, Evanston, IL 60208, USA.

3. Faculty of Infrastructure Engineering, Dalian University of Technology, Dalian 116024, China.

*These authors contributed equally to this work.
†To whom correspondence should be addressed. E-mail:jrogers@uiuc.edu

Fabrication Schematic

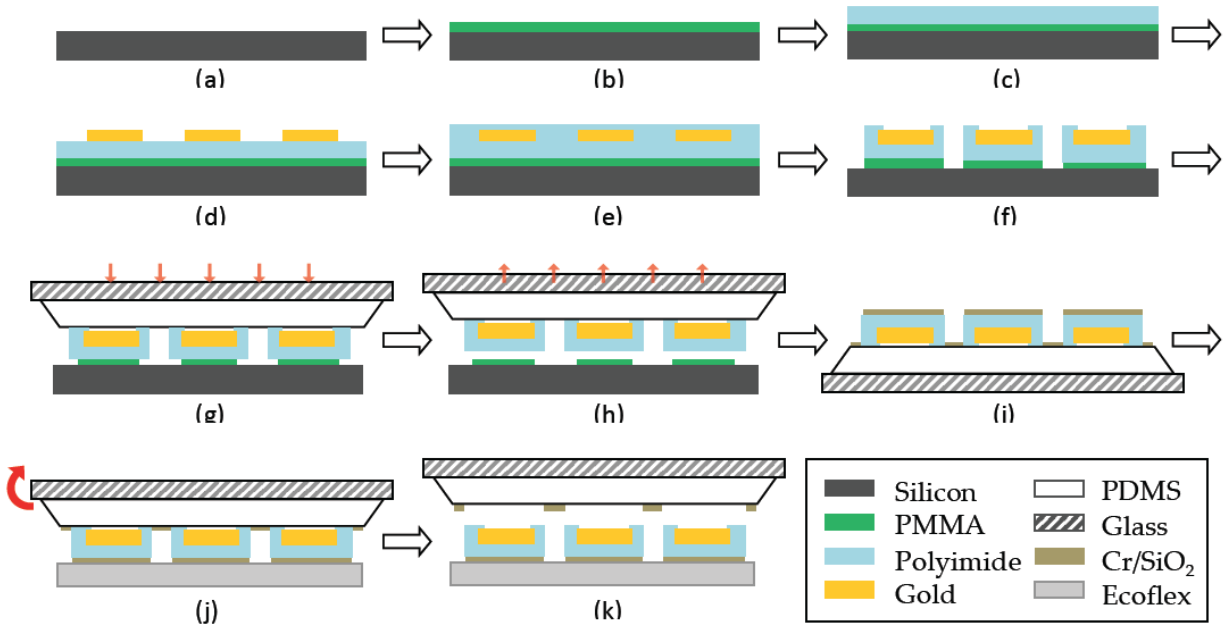

Figure S1. Schematic of the basic fabrication process. (a) Si substrate; (b) spin coat sacrificial PMMA; (c) spin coat polyimide (PI) precursor/250°C bake in inert atmosphere; (d) Au evaporation/patterning; (e) spin coat PI precursor/250°C bake in inert atmosphere; (f) O_2 RIE to expose Au electrodes and form PI mesh structure; (g) PMMA undercut in acetone/application of PDMS stamp; (h) devices transferred to PDMS stamp; (i) Cr/SiO_2 evaporated onto back of device; (j) PDMS stamp pressed onto UV exposed Ecoflex; (k) transfer completed with PDMS stamp removal.

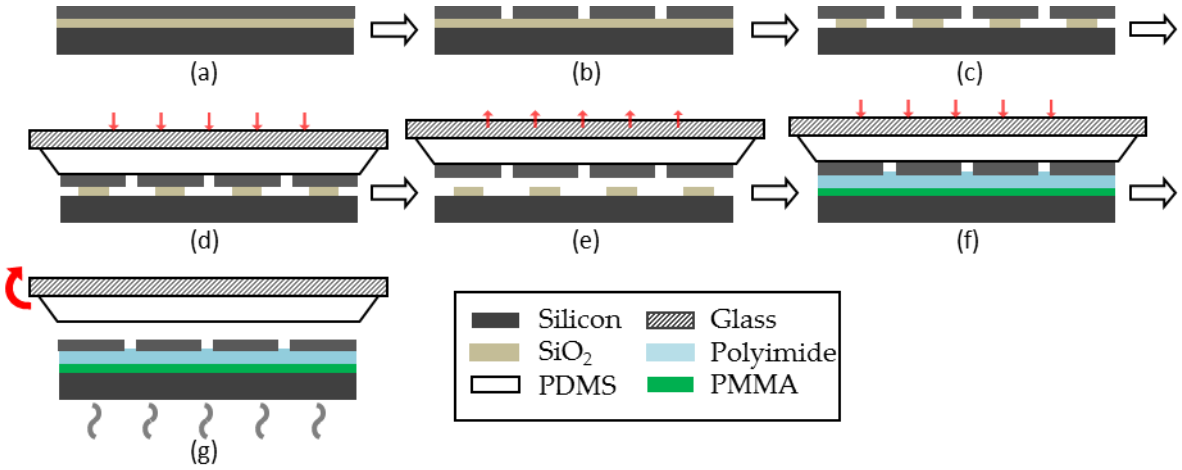

Figure S2. Schematic of silicon transfer printing. (a) silicon on insulator (SOI) substrate; (b) RIE etch release holes (3 µm) in Si layer; (c) wet etch (buffered oxide etch) of SiO_2 layer to release Si layer; (d) PDMS stamp pressed into contact with Si; (e) Si transfer to PDMS stamp upon removal; (f) PDMS stamp with transferred Si pressed onto PI layer; (g) After heating at 150°C for 4 min, Si transferred to device upon stamp removal.

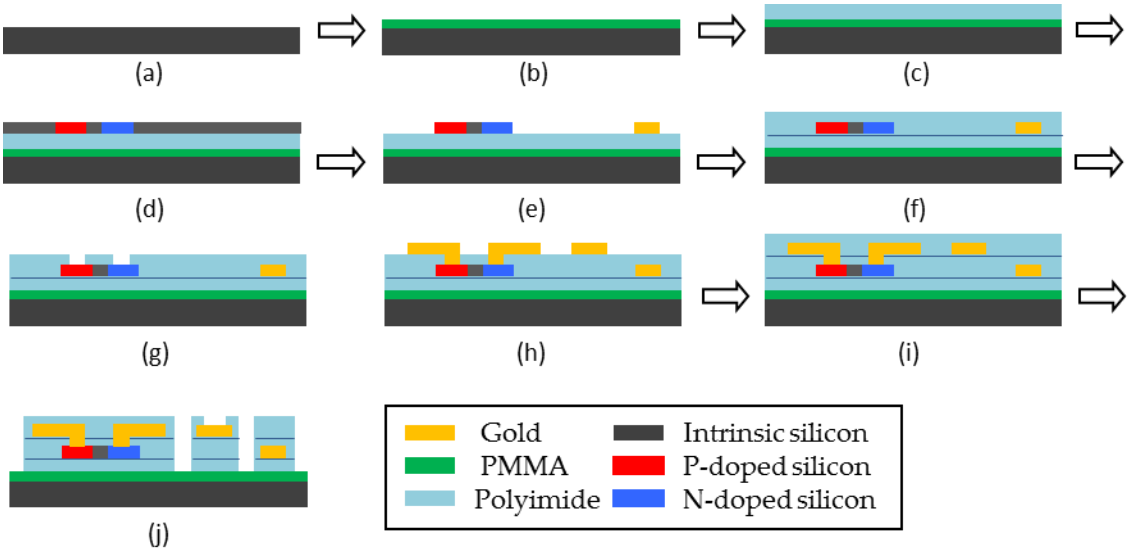

Figure S3. Schematic of the fabrication process for electrotactile stimulators. (a) silicon substrate; (b) spin coat 100 nm sacrificial PMMA; (c) spin coat/250°C bake 1.2 µm polyimide; (d) transfer of Si layer with PIN diodes (release holes not shown); (e) RIE isolation of Si nanomembrane PIN diodes and Au evaporation/patterning; (f) spin coat/250°C bake 1.2 µm polyimide; (g) contact vias for diodes formed in PI with O_2 RIE; (h) Au evaporation/patterning; (i) spin coat/250°C bake 1.2 µm polyimide; (j) O_2 RIE to form polyimide mesh structure and expose electrotactile electrodes.

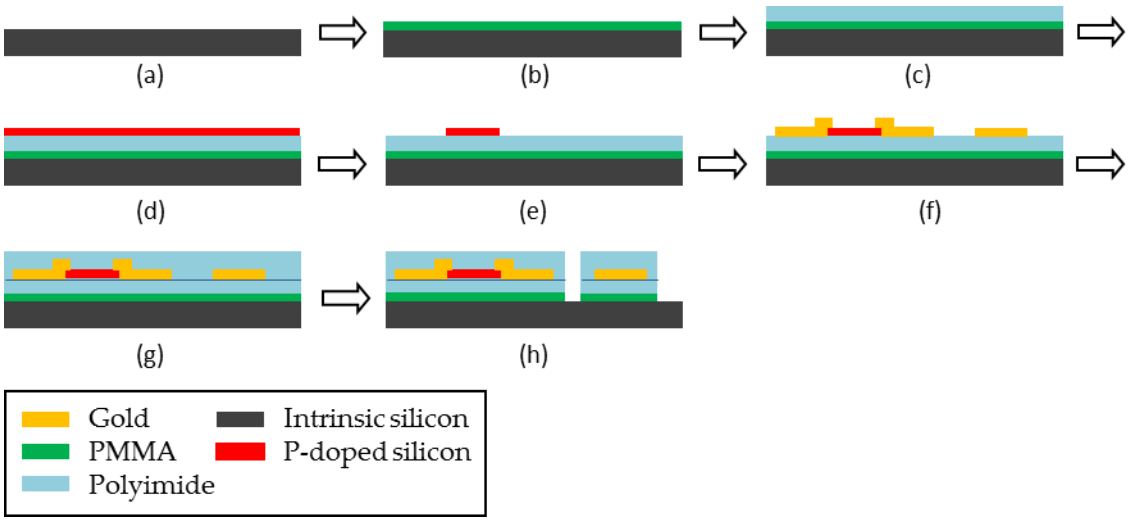

Figure S4. Schematic of the fabrication process for strain gauges. (a) silicon substrate; (b) spin coat 100 nm sacrificial PMMA; (c) spin coat/250°C bake 1.2 µm polyimide; (d) transfer of p-doped Si (release holes not shown); (e) RIE isolation of Si strain gauge nanomembranes; (f) Au evaporation/patterning; (g) spin coat/250°C bake 1.2 µm polyimide; (h) O_2 RIE to form polyimide mesh structure.

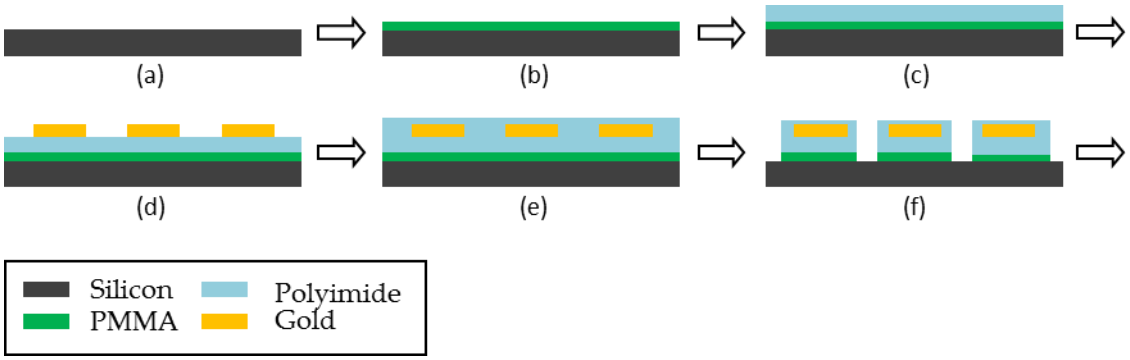

Figure S5. Schematic of the fabrication process for tactile electrodes. (a) silicon substrate; (b) spin coat 100 nm sacrificial PMMA; (c) spin coat/250°C bake 1.2 µm polyimide; (d) Au evaporation/patterning; (e) spin coat/250°C bake 1.2 µm polyimide; (f) O_2 RIE to form polyimide mesh structure.

Fabrication Steps

1. Electrotactile arrays:

1.1. Cut 1'x1' SOI wafers ((110), 300nm Si) and clean with acetone and IPA.

1.2. Form a 900nm layer of SiO_2 by PECVD as p-dope diffusion mask.

1.3. Pattern diffusion mask:

1.3.1. Pattern photoresist (PR) AZ5214: Spin coat PR AZ5214 (3000rpm, 30s), pre-bake (110°C, 1min), align mask and expose, develop with MIF327 (40s), post-bake (110°C, 3min).

1.3.2. Wet etch with buffered oxide etchant (BOE) (NH4F: HF=6:1) for 1.5 min and remove PR with acetone.

1.4. P-type doping:

1.4.1. Clean wafers with Nano-strip™ (Cyantek), place next to boron doping source, and put into furnace (1000°C) for 30min.

1.4.2. Etch SiO_2 mask completely with HF (30sec), and form another 900nm layer of SiO_2 by PECVD as n-dope diffusion mask.

1.4.3. Pattern diffusion mask: Same as step 1.3.

1.5. N-type doping:

1.5.1. Clean wafers with Nano-strip™, place next to phosphorous doping source at 1000°C for 10min.

1.5.2. Etch SiO_2 mask completely with HF (30sec).

1.6. Create holes (3μm dia., spacing 30μm) for releasing Si film:

1.6.1. Spin coat PR Shipley S1805 (3000rpm, 30s), pre-bake (110°C, 1min), align mask and expose, develop with MIF327 (9s), post-bake (110°C, 3min).

1.6.2. Etch Si with RIE (50 mtorr, 40 sccm SF6, 100 W, 1min).

1.7. Undercut oxide layer of SOI:

1.7.1. Immerse wafers in HF solution for 15~20min until the Si layer is detached from the substrate.

1.8. Pick up the Si film from the SOI wafer with a PDMS stamp.

1.9. Prepare target Si wafer:

1.9.1. Spin coat Si wafer with polymethylmethacrylate (PMMA, 3000rpm, 30s, ~100nm), cure at 180°C for 1.5min.

1.9.2. Spin coat polyimide precursor (4000rpm, 30s) and partially cure at 150°C for 40sec.

1.10. Transfer Si to target Si wafer:

1.10.1. Press the stamp into contact with the target wafer and apply force with hands for 10s.

1.10.2. Put stamp and target wafer on a hotplate at 110°C and slowly release the stamp when thermal expansion of the stamp is observed.

1.10.3. Put target wafer (now with Si film) on hotplate at 150°C for another 5min and remove PR with acetone (2 s).

1.10.4. Bake in an inert atmosphere at 250°C for 1hr.

1.11. Si diode isolation:

1.11.1. Pattern PR AZ5214.

1.11.2. Etch exposed Si with RIE (50 mtorr, 40 sccm SF6, 100 W, 1min) and strip PR with acetone.

1.12. 1st Au interconnect layer:

1.12.1. Deposit Cr (5 nm)/Au (200 nm) with electron beam evaporator.

1.12.2. Pattern PR AZ5214.

1.12.3. Wet etch Au and Cr.

1.12.4. Strip PR with acetone.

1.13. PI insulation layer with vias:

1.13.1. Spin coat polyimide precursor (4000rpm, 30s).

1.13.2. Prebake on hotplate (150°C, 5min).

1.13.3. Bake in an inert atmosphere at 250°C for 1hr.

1.13.4. Spin coat PI with PR AZ4620 (3000rpm, 30s), pre-bake (110°C, 1min), align via mask and expose, develop with 3:1 diluted MIF400 (40s).

1.13.5. Etch exposed polyimide with RIE (100W, 150mTorr, 20sccm O_2, 20min).

1.13.6. Strip PR with acetone.

1.14. 2nd Au interconnect layer:

1.14.1. Deposit Cr (10 nm)/Au (600 nm) with electron beam evaporator.

1.14.2. Pattern PR AZ5214.

1.14.3. Wet etch Au and Cr.

1.14.4. Strip PR with acetone.

1.15. Final PI encapsulation and etch:

1.15.1. Form PI layer: Same as steps 1.13.1 – 1.13.3.

1.15.2. Pattern PR AZ4620.

1.15.3. Etch exposed polyimide with RIE (100W, 150mTorr, 20sccm O_2, 50min) to form PI mesh structure.

1.15.4. Strip PR with acetone.

1.16. Transfer printing:

1.16.1. Immerse device in heated acetone bath (100°C) to undercut PMMA.

1.16.2. Press PDMS stamp into contact with the device and quickly remove to transfer device onto the stamp.

1.16.3. Deposit Cr (5 nm)/SiO_2 (20 nm) with e-beam evaporator.

1.16.4. Ultra-violet/ozone(UV-O) treat the target substrate (Ecoflex finger tube) for 4min.

1.16.5. Press the PDMS stamp onto Ecoflex and remove stamp slowly.

2. <u>Strain gauge arrays:</u>

2.1. Cut 1'x1' (110) SOI wafers (300 nm Si) and clean with acetone and IPA.

2.2. P-type doping: same as step 1.4 with a 4 min doping time.

2.3. Transfer print Si to target wafer: same as step 1.10.

2.4. Si strain gauge isolation: same as step 1.11.

2.5. Au interconnect layer: same as step 1.12.

2.6. Final encapsulation: same as step 1.15 with 30 min O_2 RIE.

2.7. Transfer printing: same as step 1.16.

3. <u>Contact sensor array:</u>

3.1. Cut 1'x1' Si wafers and clean with acetone and IPA.

3.2. Spin coat PMMA (3000 rpm, 30s) as sacrificial layer.

3.3. Form polyimide layer as substrate: Same as steps 1.13.1 – 1.13-3.

3.4. Au interconnect layer: same as step 1.12.

3.5. Final encapsulation: same as step 1.15.

3.6. Transfer printing to overlay with electrotactile electrodes: same as step 1.16.

Mechanics Modelling

Strain of the multiplexed electrotactile arrays during the flipping-over process

The elastomeric Ecoflex finger-tube with the thickness t_{sub} is flipped over twice on the finger model with the radius R_{finger}. Figure S6 illustrates a self-equilibrated, axisymmetric Ecoflex tube during the flipping-over process; AB represents the cylindrical portion in contact with the surface of plastic hand; the outer surface DE is also cylindrical; transition between the two can be approximated by a semi-circle BC (with radius R_1 to be determined in Figure S6) and a sinusoidal curve CD (with half wavelength L to be determined). For the profile shown in Figure S6, the linear elastic shell theory gives the bending energy and the membrane energy. Minimization of the total energy then gives R_1 and L. For $R_{finger} = 7.5mm$ and $t_{sub} = 500\mu m$, energy minimization gives the bending radius $R_1 = 596\mu m$ and $L = 2.47mm$ for the Poisson's ratio of Ecoflex $\nu = 0.496$. The maximum tensile and compressive strains in Ecoflex are $\varepsilon_{tensile} = 34.4\%$ and $\varepsilon_{compressive} = -49.5\%$, which agree well with the FEM results ($\varepsilon_{tensile} = 35.1\%$ and $\varepsilon_{compressive} = -46.9\%$).

The multiplexed electrotactile arrays are modeled as a composite beam with multiple layers. The bending moment and membrane force obtained from the above analytical model are imposed on the multiplexed electrotactile arrays. This gives the analytical expressions of the maximum strain in Si and Au, which are validated by FEM for relatively long Si diodes. For relatively short Si diodes, the analytical expressions overestimate the maximum strain in Si and Au.

Mechanical analysis of the tactile (pressure) sensor

The inner dot and outer ring electrodes form pairs of parallel capacitors. The capacitance change is related to the applied pressure that results in the decrease of the thickness of Ecoflex dielectric

$$\frac{\Delta C}{C_0} = \frac{P}{\overline{E}_{ecoflex} - P}, \tag{S1}$$

where $\overline{E}_{ecoflex} = 1-\nu \ E \Big/ \left[1+\nu \ \ 1-2\nu \right]$ is the effective modulus of Ecoflex dielectric under uniaxial stretching, and E=60 kPa is the Young's modulus of Ecoflex. As shown in Fig. 6d, Eq. (S1) agrees well with experiments.

For an applied tensile strain $\varepsilon_{applied}$, the strain in the Ecoflex dielectric between electrodes is related to the tensile stiffness EA_{system} of the system and tensile stiffness $EA_{\text{electrodes}}$ of the electrodes by $\varepsilon_{applied} \ EA_{\text{system}} \Big/ EA_{\text{electrodes}}$. The capacitance change of a single element of the pressure sensor array is also determined by the decrease of the thickness of the Ecoflex dielectric, and is given by

$$\frac{\Delta C}{C_0} = \frac{EA_{system}}{EA_{electrodes}} \nu \varepsilon_{applied}. \tag{S2}$$

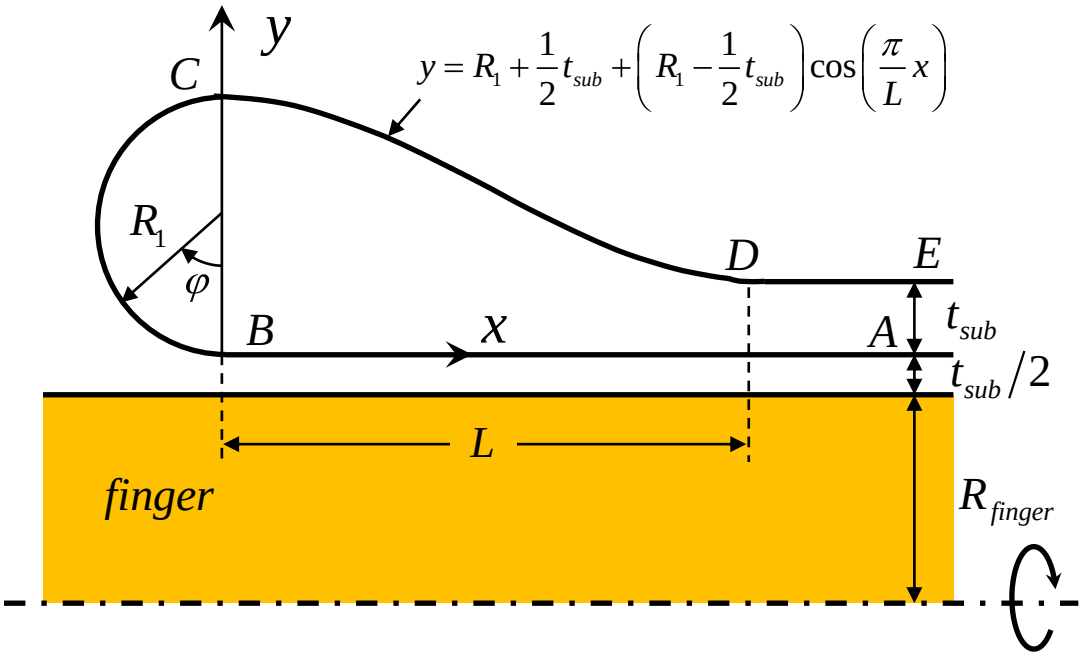

Figure S6. Schematic illustration of the flipped-over elastomeric Ecoflex tube in the plastic hand model.